Screening of Coulomb interactions in liquid dielectrics

Salman Seyedi[1], **Daniel R. Martin**[1]

[1]Department of Physics, Arizona State University, PO Box 871504, Tempe, AZ 85287-1504

Dmitry V. Matyushov[2,*]

[2]Department of Physics and School of Molecular Sciences, Arizona State University, PO Box 871504, Tempe, AZ 85287-1504

E-mail: dmitrym@asu.edu

Abstract. The interaction of charges in dielectric materials is screened by the dielectric constant of the bulk dielectric. In dielectric theories, screening is assigned to the surface charge appearing from preferential orientations of dipoles along the local field in the interface. For liquid dielectrics, such interfacial orientations are affected by the interfacial structure characterized by a separate interfacial dielectric susceptibility. We argue that dielectric properties of polar liquids should be characterized by two distinct susceptibilities responsible for local response (solvation) and long-range response (dielectric screening). We develop a microscopic model of screening showing that the standard bulk dielectric constant is responsible for screening at large distances. The potential of mean force between ions in polar liquids becomes oscillatory at short distances. Oscillations arise from the coupling of the collective longitudinal excitations of the dipoles in the bulk with the interfacial structure of the liquid around the solutes.

Keywords: dielctric screening; molecular structure; polar liquids; perturbation theory

PACS numbers: 87.15.-v, 87.15.He, 87.15.By, 87.10.Pq

Submitted to: *J. Phys.: Condens. Matter*

1. Introduction

The material formulation of the Coulomb law suggests that the potential energy of two charges, q_1 and q_2, placed in a dielectric material with the dielectric constant ϵ should be determined from the equation

$$U = \frac{q_1 q_2}{\epsilon R}. \tag{1}$$

The dielectric is then said to screen the interaction between two charges placed at distance R, lowering the interaction energy from its vacuum value $q_1 q_2/R$ to a value ϵ times smaller. While the language of interaction energy is often used in textbook electrostatics, U is in fact a potential of mean force (PMF), a free energy, as is now well understood [1, 2, 3, 4, 5, 6] and will also become clear from the discussion presented below.

Dielectric screening is assigned in theories of dielectrics to the surface charge created at the dividing dielectric surface. For instance, when an ion with the charge q is introduced in the dielectric, the surface charge of an opposite sign is placed at the cavity expelled by the ion from the dielectric material (figure 1). Maxwell thought of the surface charge as the result of deformation of the entire material made of positively and negatively charged fluids neutralizing each other [7]. The external field then deforms the material by pulling and pushing the oppositely charged liquid in opposite directions and creating opposite charges at the dividing surfaces. This view might still apply to an ionic crystal, but needs revision when molecular polar materials are concerned. The current view of interfacial dielectric polarization of polar molecular materials is that molecular dipoles are oriented by the field and predominantly point their oppositely charged ends toward the external charges. Even though they move randomly by thermal agitation, a larger fraction of molecules arrives at the interface oriented along the field thus producing an overall surface charge density of the sign opposite to the sign of the external charge [8].

The mathematics built around this picture assigns the surface charge density σ to the projection of the polarization density $\mathbf{P}$ of the material onto the unit vector $\hat{\mathbf{n}}$ normal to the dividing surface and pointing outward from the dielectric [9]: $\sigma = P_n = \hat{\mathbf{n}} \cdot \mathbf{P}$ (figure 1). The surface charge density at the cavity surrounding the charge q_1 is then $\sigma_1 = -(q_1/S)(1 - \epsilon^{-1})$, where $S = 4\pi a^2$ is the surface area of the cavity with the radius a. The electrostatic potential of charge q_1 and the potential of the opposite charge distributed over the cavity surface add up to $\phi_1 = q_1/(\epsilon r)$ at any $r > a$. This electrostatic potential then interacts with the charge q_2 with the energy $U = q_2\phi_1$, thus recovering equation (1). Importantly, the electrostatic potential in the medium is a small number produced by a nearly complete compensation of two large numbers of opposite sign: the vacuum potential and the potential of the surface charge. This mathematics puts a significant constraint on the accuracy of theoretical formalisms, which should incorporate this compensatory effect before any approximations have been introduced.

This textbook consideration, and more elaborate derivations [10], make a case for a proposal that screening of charges in the bulk of a dipolar dielectric is a surface

phenomenon dictated by the orientational structure of dipoles in the interface. If this assumption is correct, then the statistics of material's dipoles pointing their opposite ends to the external charge cannot be determined solely by bulk properties of the material and should be a function of the interfacial structure as well. While Maxwell's notion of bulk deformation still applies to ionic lattices, the focus on the interface seems to be particularly important for liquid dielectrics which respond to inserting a solute by altering their interfacial structure, both in terms of dipolar orientations and interfacial density. The goal of this article is to investigate physical consequences of this proposition and to develop a mathematical formalism to correct equation (1). Our focus here is on liquid dielectrics which, according to the picture of interfacial polarization, can build global dielectric screening through changes in the interfacial structure. We show below that, in agreement with standard expectations, the bulk dielectric constant and not interfacial structure ultimately determine the long-distance screening of charges. The interfacial structure affects screening at short distances only.

The fact that the surface charge density can be significantly modified in polar liquids compared to the standard prescriptions of dielectric theories can be established by numerical simulations of microscopic interfaces. One needs, in accord with the standard rules, the statistical average of the normal projection of the polarization density $\langle P_n \rangle$. It can be calculated from the fluctuation relation [10, 11]

$$\langle P_n \rangle = -\beta \langle \delta P_n \delta U^C \rangle, \tag{2}$$

where δU^C is the fluctuation of the Coulomb interaction between the charge and the polar medium and $\beta = (k_{\rm B}T)^{-1}$ is the inverse temperature. This fluctuation formula was indeed evaluated from molecular dynamics (MD) trajectories obtained for a model nonpolar Kihara solute and corresponding solutes carrying ionic charges [11]. The result of this calculation was the effective dielectric constant of the interface $\epsilon_{\rm int} \simeq 9$ for $a = 5$ Å. The result is obviously much lower that the dielectric constant of bulk water (TIP3P water with $\epsilon \simeq 97$ in the simulations). A low value of an effective dielectric constant around $\epsilon \simeq 5$ has long been suggested to explain ionic mobility [12, 13]. Even lower dielectric constants, ≈ 2.1, have been recently reported for water confined at the graphite surface.[14] Based on simulations, for relatively large solutes, $\simeq 10$ Åin diameter, the interfacial dielectric constant was calculated to be independent of the charge placed at the solute center.[11] The low values of $\epsilon_{\rm int}$ might therefore characterize the interfacial structure and not the pulling force of the ionic charge.

The question we address here is what is the dielectric constant that should be used in equation (1) at distances of the nanometer scale. We develop an analytical theory of microscopic screening by a polar liquid and perform molecular dynamics simulations of model solutes in SPC/E water. The main result of the proposed theory is the fluctuation relation for the screening between the charges in the dielectric and the perturbation theory formulated in terms of microscopic pair correlation functions. It casts the screening of charges by a polar liquid in terms of the structure factor of the longitudinal collective excitations of the liquid dipoles. The exact result of this

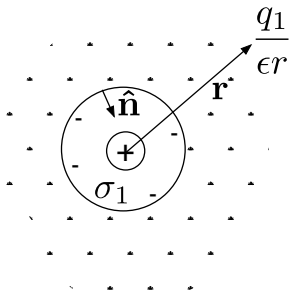

Figure 1: Schematic representation of screening of charge q_1 by the dielectric with the dielectric constant ϵ. Surface charge with the charge density $\sigma_1 = P_n = \mathbf{P} \cdot \hat{\mathbf{n}}$ develops at the dividing surface. The electrostatic potentials produced by the charge q_1 and by the oppositely charged surface charge density σ_1 add up to $q_1/(\epsilon r)$ inside the dielectric.

consideration is the following relation

$$U(R) = \frac{q_1 q_2}{\epsilon R} - q_1 q_2 \sum_n I^{(n)}(R). \tag{3}$$

Here, the first term is the standard dielectric result in (1). The second term is the sum over all longitudinal collective excitations of the liquid represented by the poles of the corresponding longitudinal structure factor. These excitations of the bulk liquid dielectric are coupled to the interfacial structure of the solutes to create oscillations of the PMF around the long-distance dielectric result given by (1). In contrast to screening by free charges in plasmas, where plasmon excitations are quasiparticles with the lifetime significantly exceeding the oscillation period, longitudinal excitations in polar liquids (dipolarons [15, 16, 17, 18, 19]) are overdamped. The qualitative outcome of the theory is that their overall effect is represented by exponentially decaying oscillations with the decay length Λ and the oscillation wavevector $k_{\max}$ given by the first maximum of the polarization structure factor

$$\sum_n I^{(n)}(R) \propto e^{-R/\Lambda} \cos\left(k_{\max} R\right). \tag{4}$$

Most simulations of the PMF between ions in solution have been performed for small ions typically used as electrolytes [4, 20, 21]. The effect of the molecular structure of water on ion pairing is clearly seen in energetic stabilization of contact and solvent-separated ion-pair configurations. The well-defined molecular structure of water around small ions is expected to alter at a nanometer cross-over length-scale [22, 23], asymptotically approaching the structure at flat interface. While this cross-over is usually understood in terms of changes in the density profile and shell compressibility [24], the electrostatic interfacial properties are affected as well [25, 26]. As an example of a dramatic crossover in electrostatic properties, we show in figure 2 the change of the variance of the solvent field E_s at the center of a spherical solute with the solute size. Applying the linear response approximation, one anticipates that the variance of the

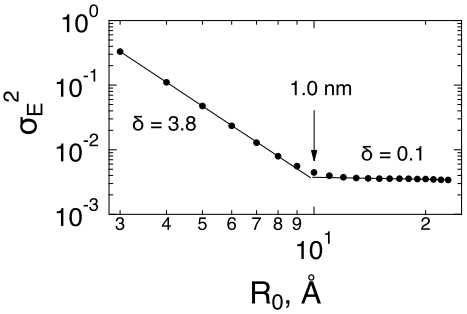

Figure 2: Variance of the electric field of SPC/E water at the center of a set of non-polar Kihara solutes with varying size R_0. The solid lines show the fitting of the data with the power law $\sigma_E^2 \propto R_0^{-\delta}$. The resulting values of δ for smaller and larger solutes are indicated in the plot. The simulations [26] are done for the Kihara solutes of varying size with the solute-solvent interaction energy $\epsilon_{\rm LJ} = 0.65$ kJ/mol [equation (32)].

solvent field scales as inverse cube [25] of the solute radius R_0

$$\sigma_E^2 = \beta\sigma^3\langle(\delta E_s)^2\rangle_0 \propto (\sigma/R_0)^3, \tag{5}$$

where the solvent diameter σ is used to produce the dimensionless quantity σ_E^2. For solute radii below $\simeq$ 1 nm, the molecular dynamics (MD) simulations [26] show the power law $\sigma_E^2 \propto R_0^{-\delta}$ with $\delta = 3.8$ not too far from the expectation. In contrast, there is a sharp cross-over in scaling at $R_0 \simeq 1$ nm, when the exponent changes to $\delta = 0.1$, i.e., essentially no decay of σ_E^2 with the growing solute size. These results are reported here based on previously produced trajectories [26] for Kihara solutes [27, 28] of varying size. This model solute combines a hard-sphere core with the radius $r_{\rm HS}$ with a Lennard-Jones layer of thickness σ_{0s} at the surface (see the discussion of the simulation protocol below and, in particular, the interaction potential in (32)). The radii reported in figure 2, $R_0 = r_{\rm HS} + \sigma_{0s}$, are altered by changing $r_{\rm HS}$.

The slowing down of the decay of the field variance with increasing solute size is caused by softening of the interface [22], thus allowing stronger fluctuations compensating for an increased size. This crossover does not rule out further crossovers as the size of the solute increases, as we anticipate, but cannot prove with the present computational capabilities. Independently of the long-distance asymptote of σ_E^2, the appearance of a soft, fluctuating interface raises the question of its coupling with the bulk dipolaron excitations responsible for oscillations in electrostatic screening [19] [Eqs. (3) and (4)]. For small ions, screening is mostly driven by dielectric laws [2] and the structure of the hydration shell is insignificant except at the contact configuration [4]. One wonders how extending the size of the solute and changing the density of the hydration layer affect this outcome. Here we report new simulations of the Kihara solutes in SPC/E water [26] to address these questions. We study how dipolaron excitations in the bulk couple to the interfacial structure and how does this coupling affect oscillations of microscopic dielectric screening. We find that increasing density of

the hydration layer, by increasing the solute-solvent attraction, significantly amplifies the PMF oscillations. On the other hand, increasing the size of the solute, beyond the cross-over region in figure 2, reduces the oscillations amplitude and leads to a faster approach to the dielectric limit. In other words, softening of the nanometer-scale interface leads to a faster approach to the continuum limit for ionic screening.

2. Fluctuation relations

We now consider two charges, q_1 and q_2, at the distance R immersed in a polar material. Each charge is represented by a repulsive sphere with the radius a defined more precisely below. The total free energy of this system of charges is the sum of their vacuum interaction energy and the free energy of polarizing the dielectric F_s

$$F = \frac{q_1 q_2}{R} + F_s. \tag{6}$$

The solvation free energy can be found by thermodynamic integration in terms of the λ-scaled Coulomb interaction energy u_q with the solvent [29]

$$F_s = \int_0^1 d\lambda \langle u_q \rangle_\lambda \tag{7}$$

where the average $\langle u_q \rangle_\lambda$ is taken with the statistical ensemble in equilibrium with the solute-solvent potential λu_q. One can choose any value $0 \leq \lambda_0 \leq 1$ as the reference system and perform a series expansion in terms of the deviation $(\lambda - \lambda_0)u_q$. The result is

$$F_s = \langle u_q \rangle_{\lambda_0} + \left(\lambda_0 - \tfrac{1}{2}\right) \beta \langle (\delta u_q)^2 \rangle_{\lambda_0} + \dots. \tag{8}$$

Here, $\delta u_q = u_q - \langle u_q \rangle_{\lambda_0}$ and the interaction energy u_q between the charges and the dielectric is given in terms of the electrostatic potentials ϕ_{si} created by the dielectric at the positions of charges q_i, $i = 1, 2$

$$u_q = q_1 \phi_{s1} + q_2 \phi_{s2}. \tag{9}$$

In the linear response approximation [30, 31], the infinite expansion is truncated after the second term in (8). Further, the statistical average $\langle \dots \rangle_{\lambda_0}$ can be performed for the liquid either in equilibrium with u_q and charges q_i or in equilibrium with the repulsive core potentials of the solutes at $q_i = 0$, or for any charge state in between [32]. Previous studies [30, 31, 33, 11] have shown that linear response is satisfied exceptionally well when the ionic radius a is sufficiently large to avoid strong interactions between the charges and the dipoles of the medium. We will assume first that this approximation holds and show below that it is indeed satisfied when tested against numerical simulations. In the case of $\lambda_0 = 0$ we have $q_i = 0$ and $\langle u_q \rangle_0 = 0$ (with slight deviations from this rule found for hydration [34, 35]). This reference configuration is adopted here for both the analytical derivation and for the numerical simulations

discussed below. The solvation free energy F_s is then given by the variance of the interaction energy

$$F_s = -(\beta/2)\langle(\delta u_q)^2\rangle, \tag{10}$$

where we put $\langle\dots\rangle_0 = \langle\dots\rangle$ for brevity.

The variance of u_q splits into self terms, representing solvation free energies of individual charges, and the cross term modifying their interaction due to the screening by the polar material. Combining the cross terms with the vacuum interaction energy, we obtain the following formula for the screened interaction energy (PMF) between the charges [36]

$$U(R) = q_1 q_2 \left[R^{-1} - \beta\langle\delta\phi_{s1}\delta\phi_{s2}\rangle\right]. \tag{11}$$

Equation (11) is the starting point for our theoretical development. For the rest of our discussion we put $q_1 = q_2 = e$, where e is the elementary charge.

Before we proceed to the formal theory, it is useful to anticipate the result when the standard dielectric theory applies. It is easy to see that (1) is recovered when one assumes for the potential cross correlation

$$\beta\langle\delta\phi_{s1}\delta\phi_{s2}\rangle = 4\pi\chi^L R^{-1}, \tag{12}$$

where $4\pi\chi^L = 1-\epsilon^{-1}$ is the longitudinal susceptibility of a polar material [17]. According to the standard expectation of the theory of polar liquids [37], spherical ions interact with the longitudinal polarization of a dipolar liquid with the susceptibility χ^L in the macroscopic limit of long-wavelength polarization excitations. The theory, therefore, must be able to produce this limit when only the long-ranged macroscopic polarization of the medium is accounted for. The formalism developed next satisfies this expectation.

3. Perturbation theory

If the average $\langle\dots\rangle$ in (11) is treated as an ensemble average over the configurations of a polar liquid around two uncharged cavities with the radii a, the calculation of the cross correlation becomes a standard perturbation problem of liquid state theories [38]. One can write the cross correlation in terms of the solute-solvent and solvent-solvent distribution functions as follows

$$\begin{aligned}\langle\delta\phi_s\delta\phi_s\rangle &= \rho\int d1\phi_s(1)\phi_s(1)g_{0s}(r_1)\\ &+ \rho^2\int d1d2\phi_s(1)\phi_s(2)g_{0s}(r_1)g_{0s}(r_2)h_{ss}(12),\end{aligned} \tag{13}$$

where $\rho = N/V$ is the number density of a polar liquid and

$$\phi_s(1) = -\frac{\mathbf{m}_1\cdot\hat{\mathbf{r}}_\mathbf{1}}{r_1^2} \tag{14}$$

is the electrostatic potential of liquid's dipole $\mathbf{m}_1$ at the position $\mathbf{r}_1$ in the liquid, $\hat{\mathbf{r}}_1 = \mathbf{r}_1/r_1$. The positions and orientations of the liquid dipoles are combined into single

indexes such as $(1) = (\mathbf{r}, \boldsymbol{\omega}_1)$ and $d1 = d\mathbf{r}d\boldsymbol{\omega}_1/(4\pi)$. We note also that $\langle\phi_s\rangle = 0$ when no preferential orientations of liquid's dipoles is anticipated around an uncharged repulsive core of the solute. Further, the Kirkwood superposition approximation [38, 29] has been applied to the second term in (13) to represent the three-particle solute-solvent-solvent distribution function as the product of the solute-solvent pair distribution function $g_{0s}(r)$ and the solvent-solvent pair correlation function $h_{ss}(12)$. The latter depends on both the distance between two molecules in the liquid r_{12} and their orientations $\boldsymbol{\omega}_1$ and $\boldsymbol{\omega}_2$.

Superposition approximation[39][40]

MSA solutions[41, 42]

One can use Fourier transform to re-write (13) in reciprocal space. The transformation to reciprocal space allows one to eliminate the space convolution in the second summand in (13) and present the result in terms of k-space structure factors describing collective fluctuations in the liquid. The details of the derivation are given in the supplementary material (SM) and the result of this derivation is the sum of two terms, $I_1(R)$ and $I_2(R)$, representing the corresponding summands in (13) as one-dimensional k-integrals

$$I(R) = \beta\langle\delta\phi_{s1}\delta\phi_{s2}\rangle = I_1(R) + I_2(R), \tag{15}$$

where

$$\begin{aligned} I_1(R) &= \frac{6y}{\pi}\int_0^\infty dk f_{0s}(k) j_0(kR), \\ I_2(R) &= \frac{6y}{\pi}\int_0^\infty dk f_{0s}(k)^2 j_0(kR)\left[S^L(k) - 1\right]. \end{aligned} \tag{16}$$

Here, $y = (4\pi/9)\beta\rho m^2$ is the standard polarity parameter of the theory of polar liquids [38, 43], $j_n(x)$ is the spherical Bessel function of nth order [44], and $f_{0s}(k)$ appears as a result of Fourier transforming $\phi_s(1)g_{0s}(r_1)$. It is given by the relation

$$f_{0s}(k) = k\int_0^\infty dr j_1(kr) g_{0s}(r), \tag{17}$$

which is a special case of the Hankel transform [43]. Further, $S^L(k)$ in (16) is the longitudinal structure factor of a polar liquid [17, 45], which describes correlated fluctuation of the reciprocal-space polarization density projected on the direction of the wavevector $\hat{\mathbf{k}} = \mathbf{k}/k$

$$\tilde{P}^L(\mathbf{k}) = \sum_j (\mathbf{m}_j \cdot \hat{\mathbf{k}})\, e^{i\mathbf{k}\cdot\mathbf{r}_j}, \tag{18}$$

where the sum runs over all dipoles $\mathbf{m}_j$ in the liquid with their positions at $\mathbf{r}_j$. The structure factor is a scaled variance of this collective variable given as

$$S^L(k) = \frac{3}{Nm^2}\langle\tilde{P}^L(\mathbf{k})\tilde{P}^L(-\mathbf{k})\rangle. \tag{19}$$

The long-wavelength limit of the structure factor is related to the longitudinal susceptibility of a dielectric through the dimensionless density of dipoles in the liquid

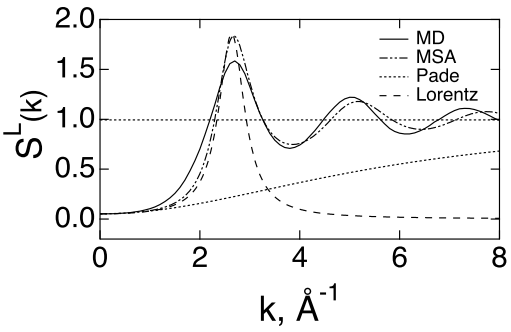

Figure 3: $S^L(k)$ for SPC/E water at $T = 300$ K from molecular dynamics simulations (MD) and from the MSA solution for dipolar hard spheres [46] in (28) (MSA). The dotted line refers to the Padé form in (25) ($\Lambda = 0.17$ Å) and the dashed line marks the Lorentz approximation [equation (26)]. The horizontal dotted line marks the $k \to \infty$ limit $S^L(\infty) \to 1$.

$y = (4\pi/9)\beta m^2 \rho$ by the following relation

$$3yS^L(0) = 4\pi\chi^L. \tag{20}$$

The opposite limit of $S^L(k)$ at $k \to \infty$ corresponds to disappearance of correlations between different dipoles in the liquid, which leads to $S^L(\infty) = 1$. Both limits are illustrated in figure 3 for SPC/E water from our simulations discussed in more detail below.

Equations (15) and (16) is a formally exact solution for the electrostatic potential cross-correlation within the limits of the linear response approximation and the Kirkwood anzatz [29] for the triple solute-solvent-solvent correlation function. We also neglect all multipoles higher than the dipole from the response of the liquid. Our simulations below show that this approximation is adequate for water in contact with relatively large solutes considered here.

The first summand in (15), $I_1(R)$, describes fluctuations of the potential at two ions produced by rotations and translations of a single molecule in the liquid. The second term, $I_2(R)$, corresponds to correlated thermal motions of two molecules. The interaction of a liquid dipole with the first charge is propagated through the liquid dipole-dipole correlations to the second dipole and then to the second charge. The function $f_{0s}(k)$ reflects the local structure of the liquid around each solute thus coupling the screening excitations of the bulk with the interfacial structure. It has an important property of $f_{0s}(0) = 1$ (see below) and scales at large k as $\exp[ika]$. This latter property allows one to convert $I_i(R)$ into the residue integrals in the complex k-space. The integral $I_1(R)$ is calculated exactly as $I_1(R) = 3y/R$ if only the pole at $k = 0$ is accounted for. The same applies to the $k = 0$ pole of $I_2(R)$. Given that we assume $R > 2a$, the $k = 0$ pole produces the result $I_2^{(0)}(R) = (3y/R)(S^L(0) - 1)$. The rest of the contour integral in the complex k-space is given by residues of $S^L(k) - 1$ at complex poles k_n. The final

result is

$$I(R) = R^{-1}\left(1 - \epsilon^{-1}\right) + \sum_n I^{(n)}(R). \tag{21}$$

This form can be substituted to equation (11) with the result for the interaction of two ions given by (3) where also the physical meaning of the microscopic screening terms $I^{(n)}(R)$ is discussed [equation (4)].

A significant advantage of the result in (3) is that it incorporates the cancellation of two large terms from the vacuum Coulomb interaction of the charges and its screening by surface charges of the dielectric as the zero-order term, thus avoiding errors from incorporating approximations into each of the components. The corrections to the continuum limit arise from longitudinal collective excitations in the polar liquid coupled to the interfacial structure of each solute. This is a physically attractive picture, which might extend beyond the derivation presented here. We explore physical consequences of it in terms of an analytical solution when the poles of the longitudinal structure factor can be well defined.

Before we turn to this next step, it is useful to identify the approximations made in deriving (21). First, we have assumed that there is no specific orientational structure of the solvent dipoles around a nonpolar solute carrying zero charge. This is a reasonable approximation in most cases, although water dipoles attend preferential orientations around nonpolar solutes.[47] This pattern, also found for SPC/E water employed here, tends to diminish when more accurate force fields are used [35]. Second, the structure factor $S^L(k)$ in (16) refers to the reference system, which is the polar liquid with inserted nonpolar repulsive cores of the solutes. Since the dielectric constant is affected by solution compared to the bulk, particularly for electrolytes [20], the ability to use the structure factor for bulk liquid needs to be tested. We in fact have done this test in our simulations discussed below and have shown that at the concentrations used in our calculations the bulk and solution structure factors are nearly identical (figure S4 in the SM). We have also tested the sensitivity of the sum over the poles, the second summand in (21), to the dielectric constant and found it relatively low. The use of the bulk structure factor $S^L(k)$ in (16) is therefore justified and we now proceed to using our analytical approximation to calculate the sum over the dipolaron excitations in the liquid.

4. Analytical solution

In order to study the behavior of $f_{0s}(k)$ in (17), we will follow here the procedure analogous to that adopted in the perturbation theory of nonpolar (Lennard-Jones) fluids. The theory of nonpolar fluids [48] starts with the observation that the Boltzmann factor, $e(r) = \exp[-\beta u(r)]$, of the intermolecular liquid potential $u(r)$ changes sharply over a short range of distances. This allows one to formulate a perturbation theory in terms of short-ranged "blip functions". Following this general framework, we consider the Boltzmann factor of the reference solute-solvent interaction potential $u_{0s}(r)$, which is

mostly repulsive and is responsible for the formation of the solute cavity with the radius a. The corresponding Boltzmann function, $e_{0s}(r) = \exp[-\beta u_{0s}(r)]$, of the solute-solvent distance r, changes between zero inside the repulsive core of the solute and unity inside the liquid. Figure 4 (dash-dotted line) shows $e_{0s}(r)$ calculated for the solute-water isotropic interaction potential given in the Kihara form [27] [equation (32)] and used in our numerical simulations discussed below. A sharp growth of $e_{0s}(r)$ implies that one can approximate its derivative by a delta-function [29]: $e'_{0s}(r) \simeq \delta(r-a)$, which also provides the definition of the cavity radius a as the position of the maximum of e'_{0s}.

We now re-write (17) in the form involving the derivative of the ion-liquid distribution function

$$f_{0s}(k) = \int_0^\infty dr j_0(kr) g'_{0s}(r). \tag{22}$$

From this equation, one gets at $k = 0$ the following boundary condition $f_{0s}(0) = g_{0s}(\infty) - g_{0s}(0) = 1$. We next note that $g_{0s}(r) = e_{0s}(r)y_{0s}(r)$, where $y_{0s}(r)$ is a smooth function.[29] One therefore can put

$$g'_{0s}(r) \simeq e'_{0s}(r)y_{0s}(r). \tag{23}$$

Figure 4 compares $e'_{0s}(r)$ with $g'_{0s}(r)$ obtained from MD simulations. One can see that $g'_{0s}(r)$ follows the shape of $e'_{0s}(r)$ at the lower value of the solute-solvent Lennard-Jones attraction energy $\epsilon_{\rm LJ}$, thus suggesting that $y(r)$ is nearly constant in the range of r-values where the spikes of these functions occur. As the attraction increases and the interface becomes more structured, the peak of $g'_{0s}(r)$ shifts to larger distances. Nevertheless, the approximation of $g'_{0s}(r)$ with a positive and negative blips turns out to be quite accurate for modeling $f_{0s}(k)$ at all parameters studied here.

Given that e'_{0s} involves positive and negative blips (figure 4), it can be represented by a sum of two delta-functions positioned at $r = a$ and $r = b$ and carrying positive and negative amplitudes. This transforms $f_{0s}(r)$ to the form

$$f_{0s}(k) = cj_0(ka) + (1-c)j_0(kb), \tag{24}$$

where b is the position of the negative blip and the coefficients in front of the spherical Bessel functions are chosen to satisfy the condition $f_{0s}(0) = 1$. The fit of this function to $f_{0s}(k)$ obtained by numerical integration in (22) is given in the SM. For our discussion here we only need to know that $f_{0s}(k)^2$ in the integral $I_2(R)$ in (16) scales at most as $e^{\pm 2ibk}$ and can perform the residue integration under the assumption $R > 2b$.

The positions of singularities of $S^L(k)$ in the complex k-plane are generally unknown and we resort here to two approximations. We first apply the Ornstein-Zernike approximate based on the known expansion of $S^L(k)$ at low wavevectors [29]. According to the Ornstein-Zernike equation, $S^L(k) = \left[1 + (\rho/3)c^L(k)\right]^{-1}$, where $c^L(k)$ is the direct correlation function propagating the longitudinal polarization through the liquid [46, 29]. The expansion $c^L(k)$ in powers of k results in a vanishing linear term such that $S^L(k)^{-1}$ becomes a linear function of k^2. One therefore can approximate $S^L(k)$ with the Padé

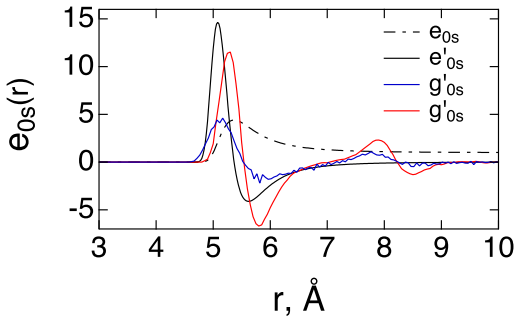

Figure 4: Boltzmann factor $e_{0s}(r)$ and its derivative $e'_{0s}(r)$ for the Kihara potential describing the solute-solvent isotropic interaction. $g'_{0s}(r)$ obtained from molecular dynamics simulations are shown at $\epsilon_{\rm LJ} = 0.65$ kJ/mol (blue) and 3.7 kJ/mol (red). The position of the positive spike of $e'_{0s}(r)$ defines the cavity radius a, which is very close to $R_0 = r_{\rm HS} + \sigma_{0s} = 5$ Å for the Kihara solutes studied here [equation (32)].

form as

$$S^L(k) = \frac{S^L(0) + \Lambda^2 k^2}{1 + \Lambda^2 k^2}, \tag{25}$$

where $\Lambda = 0.17$ Å is found from the slope of $S^L(k)^{-1}$ vs k^2 for SPC/E water (figure S5 in SM). This representation of $S^L(k)$ is not very reliable (figure 3). A better approximation can be reached in terms of the Lorenzian function with the maximum coinciding with the $k_{\rm max}$ of the simulated $S^L(k)$. Since $S^L(k)$ has to be a symmetric function of k, $S^L(k) = S^L(-k)$, the following functionality yields a more reasonable approximation (figure 3)

$$S^L(k) = \tfrac{1}{2} S^L(0) \left[\frac{k_{\rm max}^2 + \kappa^2}{(k - k_{\rm max})^2 + \kappa^2} + \frac{k_{\rm max}^2 + \kappa^2}{(k + k_{\rm max})^2 + \kappa^2} \right]. \tag{26}$$

This function has two poles in the upper-half k-plane: $k_1 = k_{\rm max} + i\kappa$ and $k_2 = -k_{\rm max} + i\kappa$. The sum over these poles results in

$$\begin{aligned} \sum_n I^{(n)}(R) =& \frac{k_{\rm max}^2 + \kappa^2}{2\kappa R} \left(1 - \frac{1}{\epsilon}\right) \\ & {\rm Im} \sum_{n=1,2} k_n^{-1} f_{0s}(k_n)^2 e^{iRk_n}. \end{aligned} \tag{27}$$

The overdamped dipolar excitations in the polar liquid produce an exponentially decaying screening, not unlike the Debye-Hückel screening by plasmon excitations in electrolytes [equation (4)]. The fitting of (26) to the simulation data produces $k_{\rm max} = 2.6$ Å^{-1} and the screening length $\Lambda = \kappa^{-1} = 3.2$ Å, both consistent with the diameter of the water molecule $\sigma \simeq 2.8 - 2.9$ Å ($2\pi/k_{\rm max} = 2.4$ Å).

The mean-spherical approximation (MSA) for dipolar fluids [46] provides a next step for improving the analytical solution. This exact solution of the Ornstein-Zernike equation with the MSA closure yields the longitudinal structure factor in terms of the

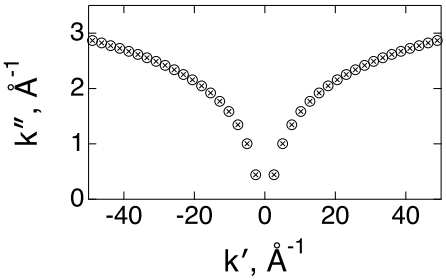

Figure 5: Poles $k_n = k'_n + ik''_n$ of the MSA longitudinal structure factor [equation (28)] in the upper half-plane of the complex k-plane: $\left|Q(\kappa^L k_n, \xi^L)\right|^2 = 0$. The pole closest to the real axis is: $k_1 = \pm 2.61 + 0.44i$, Å^{-1}.

Baxter solution [49, 29] $Q(k, \xi^L)$ of the Percus-Yevick closure for the fluid of hard spheres

$$S^L(k) = \left|Q(\kappa^L k, \xi^L)\right|^{-2}. \tag{28}$$

Here, the longitudinal polarity parameters is found from the $k = 0$ value of the structure factor by solving the equation [46]

$$S^L(0) = \frac{(1 - 2\xi^L)^4}{(1 + 4\xi^L)^2}. \tag{29}$$

In addition, an empirical factor κ^L is introduced to provide the best fit of the analytical function to the results of simulations. This slight correction is required to reproduce a more open structure of water compared to closely packed simple fluids and results in $\kappa^L = 0.85$ for SPC/E water studied here (figure 3). Similar scaling is required for other force fields of water when fitted to the Baxter function in (28). We found $\kappa^L = 0.95$ [50] and $\kappa^L = 0.93$ [51] for TIP3P [52] and SWM4-DP [53] water, respectively. The comparison of $S^L(k)$ for the SPC/E and TIP3P water models is shown in figure S4 in the SM.

The analytical form given by (28) results in a large number of poles $k_n = \pm k'_n \pm ik''_n$ in the complex k-plane (figure 5). The pole closest to the real axis has its imaginary part corresponding to the correlation length $\Lambda \simeq (k''_1)^{-1} = 2.26$ Å, reasonably close to the Lorentzian fitting. Further, the pole $I^{(n)}$ in (27) becomes

$$I^{(n)}(R) = \frac{6y}{R}\mathrm{Re}\left[\frac{f_{0s}(k_n)^2}{k_n c'_n} e^{ik_n R}\right], \tag{30}$$

where $c'_n = (\rho/3)dc^L/dk|_{k=k_n}$.

The numerical summation over the poles shown in figure 5 is compared to both the Lorentz approximation [equation (27)] and to direct integration (figure 6). The latter is done by combining the integral $I(R)$ in (15) and (16) with the Coulomb interaction energy to obtain an integral representation for the PMF

$$U(R) = \frac{6ye^2}{\pi}\int_0^\infty dk f_{0s}(k)^2 j_0(kR)\left[(3y)^{-1} - S^L(k)\right]. \tag{31}$$

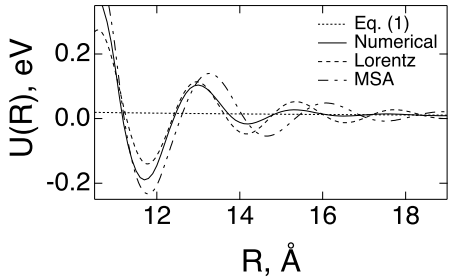

Figure 6: Direct integration in (31) (solid line) compared to the Lorentzian approximation in (27) (dashed line) and to the summation over the poles of $S^L(k)$ produced by the MSA (figure 5) (dash-dotted line). The calculations are done for two spheres with the radii 5 Å at varying distance R between their centers. The structure factor for the SPC/E water from simulations (figure 3) is used in numerical integration. The corresponding fits to the Lorentz and the MSA solutions are displayed in figure 3. The dotted line shows the dielectric result [equation (1)].

It turns out that the simplest Lorentzian form captures the main features of the PMF, and it is even superior to the summation over the poles produced by the MSA. The resulting PMF shows oscillations around the continuum solution thus producing over- and under-screening at different distances due to the molecular nature of the polar liquid.[54, 1, 2] The oscillations of the interaction energy are, however, mostly within $\sim 5-9\ k_{\rm B}T$, which is consistent with many previous simulations of ion pairing in force-field water [20, 4, 21, 55]. We now turn to direct MD simulations of the potential cross-correlation in (11).

5. Numerical simulations

Numerical MD simulations employed two solutes placed in the simulation box containing 7408 SPC/E [56] water molecules. The solute-solvent interaction potential was given by the isotropic Kihara potential [27, 28], which combines the hard-sphere repulsion characterized by the repulsion radius $r_{\rm HS}$ with a Lennard-Jones layer of the thickness σ_{0s} and the attraction energy $\epsilon_{\rm LJ}$

$$u_{0s}(r) = 4\epsilon_{\rm LJ}\left[\left(\frac{\sigma_{0s}}{r-r_{\rm HS}}\right)^{12} - \left(\frac{\sigma_{0s}}{r-r_{\rm HS}}\right)^{6}\right]. \tag{32}$$

The Kihara potential was introduced [27] to avoid too soft repulsion of the Lennard-Jones potential when applied to sufficiently large solutes.

The MD trajectories were produced with the NAMD simulation package [57] supplemented with a separate script developed to calculate the force between the Kihara solute and SPC/E water. The parameters used for the Kihara potential in this set of simulations were $r_{\rm HS} = 2$ Å, $\sigma_{0s} = 3$ Å, and $\epsilon_{\rm LJ} = 3.7$ kJ/mol. We additionally

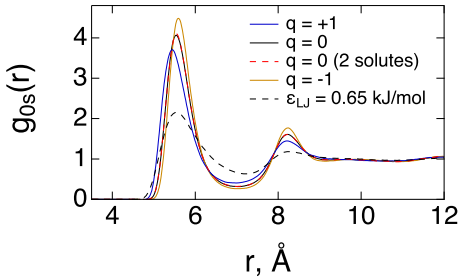

Figure 7: Solute-solvent density distribution functions $g_{0s}(r)$ calculated from MD simulations of neutral ($q = 0$) and charged ($q = \pm 1$) single Kihara solutes in SPC/E water ($r_{\rm HS} = 2$ Å). Also shown is the distribution function for a single solute in the box containing two Kihara solutes separated by the distance of $R = 20$ Å. The results shown by the solid lines refer to $\epsilon_{\rm LJ} = 3.7$ kJ/mol, while the dashed line refers to $\epsilon_{\rm LJ} = 0.65$ kJ/mol.

analyzed the trajectories obtained previously [26], which involved the variation of $r_{\rm HS}$ to produce the results shown in figure 2 and for the analysis presented below. We have also analyzed simulation data with changing solute-solvent attraction energy $\epsilon_{\rm LJ}$. Two additional values of this parameter, $\epsilon_{\rm LJ} = 0.65$ kJ/mol and $\epsilon_{\rm LJ} = 20$ kJ/mol, were used in the analysis. The former attraction energy is close to the interaction energy of the water molecules in the bulk, and it models a hydrophobic solute which does not produce a strong pull on the waters in the hydration shell [28]. The value $\epsilon_{\rm LJ} = 3.7$ kJ/mol mostly studied here is more consistent with a hydrophilic solute. Finally, the attraction at $\epsilon_{\rm LJ} = 20$ kJ/mol is so strong that it breaks water's structure and results in the condensation of the first hydration layer at the solute surface. The resulting layering is seen as a gap of zero value of the solute-solvent pair distribution between the first and second hydration layers (figure S2 in the SM).

One of the advantages of using nonpolar solutes for the calculation of the dipolar screening is that one avoids the Coulomb interactions between the charged solutes and their images in the replicas of the simulation cell, which are unavoidable in any finite-size simulations [3]. The cross-correlations

$$I(R) = \beta\langle\delta\phi_{s1}\delta\phi_{s2}\rangle \tag{33}$$

were calculated at a number of configurations with the distance between two Kihara solutes altered in the range $10 \le R \le 20$ Å. However, the ability to use the non-ionic solutes to calculate screening between ions is based on the linear response approximation, which assumes that the solvent structure remains intact for all charge state of the ion, from zero charge to the highest charge considered in this framework. In order to test this assumption we have additionally simulated single Kihara solutes in SPC/E water in neutral and charged states. For the charged solutes, the charge $q = \pm 1$ was placed at the center of the Kihara sphere. Figure 7 shows that the pair solute-solvent

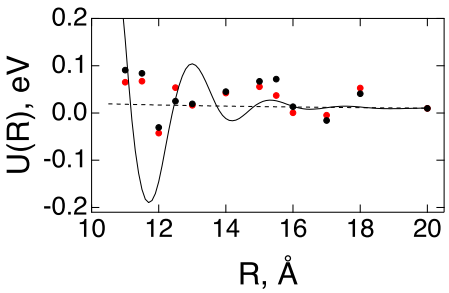

Figure 8: Results of MD simulation for two neutral Kihara solutes placed at different distances R. Black points refer to electrostatic potential created by water's partial atomic charges and the red points indicate the electrostatic potential created by the water's point dipoles. The solid line is the result of numerical integration in (31) and the dashed line is the dielectric result in (1).

distribution functions obtained for all three states are very close, in support of the linear response assumption. Further, the solute-solvent density profiles in the simulation box with two solutes are identical to single-solute distribution functions at sufficiently large separations between two spheres (figure 7, the two lines are identical on the scale of the plot). The solute-solvent density profile is in fact more strongly affected by the magnitude of the Lennard-Jones energy $\epsilon_{\rm LJ}$ in (32) than by the charge state in the range of radii considered here. The dashed line in figure 7 shows $g_{0s}(r)$ at $\epsilon_{\rm LJ} = 0.65$ kJ/mol, with a clearly less structured interface.

The results of calculations of $I(R)$ in (33) need to be combined with the direct Coulomb interaction in (11) to obtain the screened PMF. We found, in agreement with previous results [36], that this approach leads to the $R \to \infty$ asymptote shifted from zero. The reason is that the Ewald potential $\phi_{\rm E}(R)$ is shifted from the Coulomb potential [36]. The simulation results (black points in figure 8) were therefore shifted vertically to fit the analytical model (equation (31), solid line) at the largest distance studied here. We have additionally performed calculations replacing the atomic charges at the water molecules with point dipoles. These results (red points in figure 8) are very close to the charge-based calculations thus justifying the use of the dipolar density field to represent water in the analytical theory. The simulations still do not fit the analytical theory well, which we attribute to the demanding requirement to subtract two nearly-equal quantities to obtain the PMF.

We next address the question of the effect of the solute size and the density of the hydration layer on the oscillatory screening behavior of the PMF. Figure 9 shows the calculations performed according to (31) with the solute-water pair distribution functions of Kihara solutes of increasing size. A clear pattern of decreasing amplitude of the screening oscillations is seen for larger solutes. The oscillations essentially disappear beyond the size crossover shown in figure 2. The crossover to the nano-scale

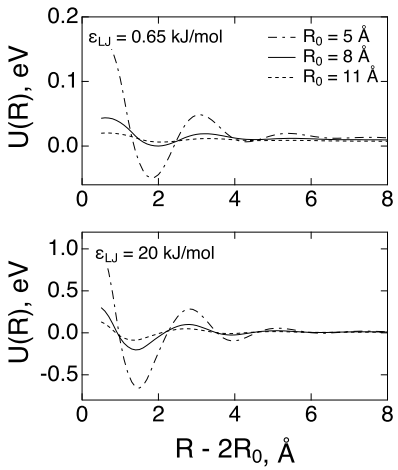

Figure 9: $U(R)$ from (31) with $S^L(k)$ for SPC/E water and $f_{0s}(k)$ calculated from solute-water distribution functions of Kihara solutes with changing size R_0. The results for two magnitudes of the solute-solvent Lenard-Jones energy $\epsilon_{\rm LJ}$ are shown.

solvation with soft solute-solvent interface also means the transition to a continuum-type electrostatic screening.

Increasing the density of the hydration shell produces an opposite effect. We achieve denser hydration layers by significantly increasing the solute-solvent Lennard-Jones attraction (the lower panel in figure 9). The value $\epsilon_{\rm LJ} = 20$ kJ/mol used to illustrate this point is somewhat unrealistic, leading to a collapse of the first hydration shell and layering between the first and second shells (see examples of the solute-solvent distribution function in figure S2 in the SM). However, this calculation produces an about order-of-magnitude increase in the amplitude of oscillations, indicating that oscillatory pattern of screening is caused by coupling of the bulk dipolarons to the interfacial structure. Increasing the structure of the hydration shell enhances the amplitude of oscillations.

6. Discussion

The textbook picture of screening of electrostatic fields in dielectrics goes back to Maxwell [7] and considers a slab of dielectric placed in an external field E_0. The external field induces bulk strain leading to surface charges. They, in turn, produce an internal electric field E_s opposing (screening) the external field. The Maxwell field $E = E_0 - E_s$ is the result of near complete cancelation between these two fields, leading to E_0 reduced by ϵ. This picture silently assumes that the dielectric is a solid and can sustain bulk stress. The dielectric constant, related to material's ability to develop this bulk stress in response to an external field, is a bulk material property.

This simple picture is bound to fail and needs to be modified for liquid dielectrics since liquids do not sustain bulk stress and any surface charge must be a surface

phenomenon. Since the dielectric constant is still a bulk material property reported by the dielectric experiment, dielectric screening needs to be described in a language disconnected from surface charges. The main question here is whether polarization of the interface and the corresponding interfacial susceptibility, which enters the local polarity response (e.g., for ion solvation), are related to dielectric screening at large (on molecular scale) distances. Not unexpected, our results show that the local response of the liquid interface is mostly unrelated to the long-distance screening. The latter is achieved in liquids by mutual correlations of the liquid dipoles in the bulk and not by the field of the surface charges.

A significant consequence of this perspective is that the bulk dielectric constant reported by the dielectric experiment applies to long-distance dielectric screening, but a local interfacial susceptibility has to be used for solvation. In practical terms, polar liquids must be characterized by at least two susceptibilities describing the surface and bulk responses separately [14]. The model solutes dissolved in the force-field water studied here provide a convincing example: their interfacial dielectric constant obtained from (2) is $\simeq 9$ [11], but the dielectric constant entering the long-distance screening is $\simeq 71$. The analytical theory presented here can be extended to liquids confined in the slab geometry since this extension is achieved at $R_0 \to \infty$ while keeping the thickness of the liquid between two solutes constant. The parameters of the theory still remain the same: the density distribution function of the interface and the longitudinal structure factor of bulk liquid.

We find that the dielectric limit of the Coulomb law in (1) is reached at long distances between the solutes, but the granularity of the polar liquid shows itself over $\simeq 0.5-1$ nm into the bulk in the form of oscillations around the dielectric solution. These oscillations are linked to the overdamped excitations in the polar liquid (dipolarons [15, 16, 17, 18, 19]) represented by the poles of the longitudinal structure factor of dipolar polarization density [58]. The excitation with the longest length of decay is responsible for the first peak of the structure factor and is mostly sufficient to reproduce the oscillatory screening calculated by numerical integration.

We conclude that dipolaron excitation responsible for the first peak in the structure factor is the main cause of the oscillatory dielectric screening and of the corresponding PMF in ion pairs. It is important to stress that previous reports of oscillatory PMF have been limited to small ions typically employed as supporting electrolytes [54, 2, 20, 4, 21]. Here we show that similar oscillations develop for dielectric screening between large solutes with the diameter of $\simeq 1$ nm.

The simulation protocol employed here is based on the fluctuation relation for the dielectric screening involving the correlation of electrostatic potential produced by the polar liquid at two solutes [equation (11)]. The advantage of this formalism is that it does not require integrating the force between the solutes over distances [21, 6]. Since the approach is based on linear response, one has the freedom to either remove the charges from the corresponding groups or keep them if needed. Nevertheless, dielectric screening is still a challenging task for simulations since subtraction of two large terms is prone to

numerical errors. A significant advantage of the theoretical approach summarized in (3) is that subtraction of two largest contributions to the PMF is achieved in the continuum limit and only microscopic corrections linked to damped dipolaron excitations require a separate calculation.

Supplementary material

See supplementary material for the simulation protocols and the data analysis.

Acknowledgments

This research was supported by the Office of Basic Energy Sciences, Division of Chemical Sciences, Geosciences, and Energy Biosciences, Department of Energy (DE-SC0015641). CPU time was provided by the National Science Foundation through XSEDE resources (TG-MCB080071).

References

[1] Shawn E Huston and Peter J Rossky. Free energies of association for the sodium-dimethyl phosphate ion pair in aqueous solution. *J. Phys. Chem.*, 93(23):7888–7895, 1989.

[2] Alexander A. Rashin. Electrostatics of ion-ion interactions in solution. *J. Phys. Chem.*, 93(11):4664–4669, 1989.

[3] Joel S Bader and David Chandler. Computer simulation study of the mean forces between ferrous and ferric ions in water. *J. Phys. Chem.*, 96(15):6423–6427, 1992.

[4] Christopher J Fennell, Alan Bizjak, Vojko Vlachy, and Ken A Dill. Ion Pairing in Molecular Simulations of Aqueous Alkali Halide Solutions. *J. Phys. Chem. B*, 113(19):6782–6791, 2009.

[5] Yun Luo, Wei Jiang, Haibo Yu, Alexander D MacKerell, and Benoît Roux. Simulation study of ion pairing in concentrated aqueous salt solutions with a polarizable force field. *Farad. Disc.*, 160(21):135–149, 2013.

[6] Daniel Trzesniak, Anna-Pitschna E. Kunz, and Wilfred F. van Gunsteren. A comparison of methods to compute the potential of mean force. *ChemPhysChem*, 8(1):162–169, 2007.

[7] J. C. Maxwell. *A Treatise on Electricity and Magnetism*, volume 1. Dover Publications, New York, 1954, sec. 63.

[8] J. D. Jackson. *Classical Electrodynamics*. Wiley, New York, 1999.

[9] L. D. Landau and E. M. Lifshitz. *Electrodynamics of Continuous Media*. Pergamon, Oxford, 1984.

[10] D. V. Matyushov. Electrostatics of liquid interfaces. *J. Chem. Phys.*, 140:224506, 2014.

[11] Mohammadhasan Dinpajooh and D. V. Matyushov. Dielectric constant of water in the interface. *J. Chem. Phys.*, 145:014504, 2016.

[12] P J Stiles, J B Hubbard, and R F Kayser. Dielectric saturation and dielectric friction in electrolyte solutions. *J. Chem. Phys.*, 77(12):6189–6196, 1982.

[13] Philip J Lenart, Arben Jusufi, and Athanassios Z Panagiotopoulos. Effective potentials for 1:1 electrolyte solutions incorporating dielectric saturation and repulsive hydration. *J. Chem. Phys.*, 126(4):044509–8, 2007.

[14] L Fumagalli, A Esfandiar, R Fabregas, S Hu, P Ares, A Janardanan, Q Yang, B Radha, T Taniguchi, K Watanabe, G Gomila, K S Novoselov, and A K Geim. Anomalously low dielectric constant of confined water. *Science*, 360(6395):1339–1342, 2018.

[15] Roberto Lobo, John E Robinson, and Sergio Rodriguez. High frequency dielectric response of dipolar liquids. *J. Chem. Phys.*, 59(11):5992–6008, 1973.

[16] E L Pollock and B J Alder. Frequency-dependent dielectric response in polar liquids. *Phys. Rev. Lett.*, 46(14):950–953, 1981.

[17] P. Madden and D. Kivelson. A consistent molecular treatment of dielectric phenomena. *Adv. Chem. Phys.*, 56:467–566, 1984.

[18] Igor P Omelyan. Temperature behavior of the frequency-dependent dielectric constant for a Stockmayer fluid. *Phys. Lett. A*, 216(1-5):211–216, 1996.

[19] I. P. Omelyan. Longitudinal wavevector- and frequency-dependent dielectric constant of the tip4p water model. *Mol. Phys.*, 93:123–135, 1998.

[20] Sergei Gavryushov. Effective Interaction Potentials for Alkali and Alkaline Earth Metal Ions in SPC/E Water and Polarization Model of Hydrated Ions. *J. Phys. Chem. B*, 110(22):10888–10895, 2006.

[21] Eva Pluhařová, Ondrej Marsalek, Burkhard Schmidt, and Pavel Jungwirth. Ab Initio Molecular Dynamics Approach to a Quantitative Description of Ion Pairing in Water. *J. Phys. Chem. Lett.*, 4(23):4177–4181, 2013.

[22] D. Chandler. Interfaces and the driving force of hydrophobic assembly. *Nature*, 437:640–647, 2005.

[23] S. Rajamani, T. M. Truskett, and S. Garde. Hydrophobic hydration from small to large lengthscales: Understanding and manipulating the crossover. *Proc. Natl. Acad. Sci.*, 102:9475–9480, 2005.

[24] S. Sarupria and S. Garde. Quantifying water density fluctuations and compressibility of hydration shells of hydrophobic solutes and proteins. *Phys. Rev. Lett.*, 103:037803, 2009.

[25] D. R. Martin and D. V. Matyushov. Electrostatic fluctuations in cavities within polar liquids and thermodynamics of polar solvation. *Phys. Rev. E*, 78:041206, 2008.

[26] D. R. Martin, A. D. Friesen, and D. V. Matyushov. Electric field inside a "Rossky cavity" in uniformly polarized water. *J. Chem. Phys.*, 135:084514, 2011.

[27] T. Kihara. Intermolecular forces and equation of state of gases. *Adv. Chem. Phys.*, 1:267–307, 1958.

[28] A. D. Friesen and D. V. Matyushov. Local polarity excess at the interface of water with a nonpolar solute. *Chem. Phys. Lett.*, 511:256–261, 2011.

[29] J.-P. Hansen and I. R. McDonald. *Theory of Simple Liquids*. Academic Press, Amsterdam, 4 edition, 2013.

[30] G Hummer and A Szabo. Calculation of freeenergy differences from computer simulations of initial and final states. *J. Chem. Phys.*, 105:2004–2010, 1996.

[31] J. Åqvist and T. Hansson. On the validity of electrostatic linear response in polar solvents. *J. Phys. Chem.*, 100:9512–9521, 1996.

[32] A. Milischuk and D. V. Matyushov. Dipole solvation: Nonlinear effects, density reorganization, and the breakdown of the Onsager saturation limit. *J. Phys. Chem. A*, 106:2146, 2002.

[33] Sowmianarayanan Rajamani, Tuhin Ghosh, and Shekhar Garde. Size dependent ion hydration, its asymmetry, and convergence to macroscopic behavior. *J. Chem. Phys.*, 120(9):4457–4466, 2004.

[34] Thomas L Beck. The influence of water interfacial potentials on ion hydration in bulk water and near interfaces. *Chem. Phys. Lett.*, 561-562:1–13, 2013.

[35] Richard C Remsing, Marcel D Baer, Gregory K Schenter, Christopher J Mundy, and John D Weeks. The Role of Broken Symmetry in Solvation of a Spherical Cavity in Classical and Quantum Water Models. *J. Phys. Chem. Lett.*, 5:2767–2774, 2014.

[36] F Figueirido, G S Del Buono, and R M Levy. On finite-size effects in computer simulations using the Ewald potential. *J. Chem. Phys.*, 103:6133–6142, 1995.

[37] J. S. Høye and G. Stell. Statistical mechanics of polar systems: Dielectric constant for dipolar fluids. *J. Chem. Phys.*, 61:562, 1974.

[38] C. G. Gray and K. E. Gubbins. *Theory of Molecular Liquids*. Clarendon Press, Oxford, 1984.

[39] S A Egorov and J L Skinner. Vibrational energy relaxation of polyatomic solutes in simple liquids

and supercritical fluids. *J. Chem. Phys.*, 112(1):275–281, 2000.

[40] Jianshu Cao, Jianlan Wu, and Shilong Yang. Calculations of nonlinear spectra of liquid Xe. I. Third-order Raman response. *J. Chem. Phys.*, 116(9):3739–3759, 2002.

[41] Derek Y. C. Chan, D. John Mitchell, and Barry W. Ninham. A model of solvent structure around ions. *J. Chem. Phys.*, 70(6):2946–2957, 1979.

[42] D Levesque, J J Weis, and G N Patey. Charged hard spheres in dipolar hard sphere solvents. A model for electrolyte solutions. *J. Chem. Phys.*, 72(3):1887–1899, 1980.

[43] G. Stell, G. N. Patey, and J. S. Høye. Dielectric constants of fluid models: Statistical mechanical theory and its quantitayive implementation. *Adv. Chem. Phys.*, 48:183–328, 1981.

[44] M. Abramowitz and I. A. Stegun, editors. *Handbook of Mathematical Functions.* Dover, New York, 1972.

[45] F. O. Raineri, H. Resat, and H. L. Friedman. Static longitudinal dielectric function of model molecular fluids. *J. Chem. Phys.*, 96:3068, 1992.

[46] M. S. Wertheim. Exact solution of the mean spherical model for fluids of hard spheres with permanent electric dipole moments. *J. Chem. Phys.*, 55:4291–4298, 1971.

[47] C. Y. Lee, J. A. McCammon, and P. J. Rossky. The structure of liquid water at an extended hydrophobic surface. *J. Chem. Phys.*, 80:4448–4455, 1984.

[48] H. C. Andersen, D. Chandler, and J. D. Weeks. Roles of repulsive and attractive forces in liquids: The equilibrium theory of classical fluids. *Adv. Chem. Phys.*, 34:105–155, 1976.

[49] R. J. Baxter. Ornstein-Zernicke relation and Percus-Yevick approximation for fluid mixtures. *J. Chem. Phys.*, 52:4559, 1970.

[50] A. A. Milischuk, D. V. Matyushov, and M. D. Newton. Activation entropy of electron transfer reactions. *Chem. Phys.*, 324:172–194, 2006.

[51] M. Dinpajooh, M. D. Newton, and D. V. Matyushov. Free energy functionals for polarization fluctuations: Pekar factor revisited. *J. Chem. Phys.*, 145:064504, 2017.

[52] William L. Jorgensen, Jayaraman Chandrasekhar, Jeffry D. Madura, Roger W. Impey, and Michael L. Klein. Comparison of simple potential functions for simulating liquid water. *J. Chem. Phys.*, 79(2):926–935, 1983.

[53] Guillaume Lamoureux and Benot Roux. Modeling induced polarization with classical Drude oscillators: Theory and molecular dynamics simulation algorithm. *J. Chem. Phys.*, 119(6):3025–3039, 2003.

[54] H Resat, M Mezei, and J A McCammon. Use of the Grand Canonical Ensemble in Potential of Mean Force Calculations. *J. Phys. Chem.*, 100(4):1426–1433, 1996.

[55] Elise Duboué-Dijon, Philip E Mason, Henry E Fischer, and Pavel Jungwirth. Hydration and Ion Pairing in Aqueous Mg 2+and Zn 2+Solutions: Force-Field Description Aided by Neutron Scattering Experiments and Ab Initio Molecular Dynamics Simulations. *J. Phys. Chem. B*, 122(13):3296–3306, 2018.

[56] H. J. C. Berendsen, J. R. Grigera, and T. P. Straatsma. The missing term in effective pair potentials. *J. Phys. Chem.*, 91:6269, 1987.

[57] James C. Phillips, Rosemary Braun, Wei Wang, James Gumbart, Emad Tajkhorshid, Elizabeth Villa, Christophe Chipot, Robert D. Skeel, Laxmikant Kalé, and Klaus Schulten. Scalable molecular dynamics with NAMD. *J. Comput. Chem.*, 26(16):1781–1802, 2005.

[58] D. Pines. *Elementary excitations in solids.* Perseus Books, 1999.